JMEPEG
https://doi.org/10.1007/s11665-024-09500-9

1059-9495/$19.00

ORIGINAL RESEARCH ARTICLE

Laser Transmission Welding of Polypropylene: Insights into Parameter Interplay, Thermal Analysis, Bonding Quality, Fracture Characteristics, and Weld Morphology

Ghulam Anwer and Bappa Acherjee

Submitted: 21 November 2023 / Revised: 27 February 2024 / Accepted: 18 March 2024

Laser transmission welding (LTW), a versatile polymer joining process utilizing laser energy, and its application to polypropylene, a widely used thermoplastic with excellent physical–mechanical properties, are relevant to various industries. This study conducts an exhaustive experimental investigation of LTW for polypropylene, aiming to deepen insights by scrutinizing parameter interplays, assessing joint quality, investigating fracture modes in welded structures, and examining fracture surface characteristics and weld morphology. Insights into polymer thermal behavior are gained through differential scanning calorimetry and thermogravimetric analysis, with carbon black enhancing thermal stability and crystallinity in polypropylene. Fracture mode analysis reveals that stronger welds align with fractures in the base polymer, while weaker bonding leads to failures at the weld interface. Residue traces at the sheared zone affirm excellent bonding. Optimal line energy control, achieved through higher laser power and faster scanning, yields both stronger and wider welds. Morphological analysis highlights strong interfacial bonding, cohesive failures, and robust weld joints, with no visible air gaps and minimal signs of decomposition in the weld interface, confirming weld integrity. This research advances the comprehension of LTW for polypropylene, providing valuable insights for practical applications.

Keywords fracture modes, laser transmission welding, polypropylene, thermal behavior, weld quality, weld morphology

1. Introduction

Polymers are everywhere in modern applications, ranging from everyday items to advanced high-tech products. They offer numerous advantages, including high strength-to-weight ratios, versatility in shaping, recyclability, corrosion resistance, and cost-effectiveness. Manufacturing complex polymer products as a single piece is not always feasible, practical, or cost-effective. Therefore, several polymer joining processes have evolved to address this issue. Laser transmission welding (LTW), introduced in the 1980s but gaining prominence in the late 1990s and early 2000s, is a relatively recent addition to the wide range of polymer joining methods (Ref 1). Its growth has been propelled by significant advancements in energy-efficient diode and fiber lasers operating at suitable wavelengths for this welding technique. While Nd:YAG lasers also operate within the suitable wavelength range for LTW, they exhibit poor energy efficiency. LTW involves placing a laser-absorbing polymer at the bottom and a transparent or translucent polymer on top of the assembly. This arrangement allows the laser to pass through the top part and be absorbed by the bottom part, generating heat. The heat generated at the interface within the bottom part is then conducted to the top polymer through contact conduction. As a result, both polymers are heated and melted at the interface, leading to fusion. Upon solidification, a strong bond is formed (Ref 2, 3). Clamping both polymers is essential to ensure close contact and sufficient contact conduction, as the top polymer heats through thermal conduction from the bottom polymer. Natural polymers are either transparent or translucent at the wavelength of the laser used for LTW (0.8-1.1 μm), and therefore, they are rendered laser-absorbing by blending with appropriate laser-absorbing pigments or dyes (Ref 3). For welding two transparent or translucent polymers, a laser-absorbing third medium in the form of ink or film is placed at the interface to absorb the laser beam and generate the heat required for welding (Ref 4). Several laser-absorbing agents like Clearweld®, Lumogen® dyes, and additives have been developed for welding transparent polymers. For laser welding of polymers without the use of laser-absorbing additives, lasers are used whose wavelength (1.6-2.1 μm) is readily absorbed by the polymers used for welding (Ref 5). LTW provides numerous advantages, such as being a non-contact, precise, and flexible process that can be highly automated, leading to high productivity, cost-effectiveness, and consistent quality. However, it typically involves a higher initial investment compared to other polymer joining methods (Ref 6). LTW has diverse applications in industries, such as automotive, medical devices, electronics, micro-technology, textiles, and packaging. Its cost-effectiveness is evident in various applications within the cost-sensitive automotive sector, producing various components like filters, connectors, and taillights (Ref 7, 8).

Ghulam Anwer and **Bappa Acherjee**, Department of Production and Industrial Engineering, Birla Institute of Technology: Mesra, Ranchi 835215, India. Contact e-mails: bappa.rana@gmail.com and a.bappa@yahoo.com.

Published online: 30 April 2024

LTW has garnered significant research interest due to its potential to revolutionize polymer welding. Many researchers have put their efforts into investigating various aspects of LTW through experimental and numerical studies. Kagan and Pinho Ref 9 investigated the mechanical performance of shear and butt joint-welded nylon 6 plastic, finding that increasing fiberglass content enhanced weld width and tensile strength but reduced strength at the weld zone. Kocheny et al. Ref 10 investigated the effect of moisture on LTW and found that it has no significant effect on the mechanical performance of the weld. A similar study on polyamide (Ref 11) showed laser welding to be efficient for wet materials, with moisture acting as a plasticizer, enhancing ductility. Prabhakaran et al. Ref 12 investigated T-joint welding of 30% glass-reinforced nylon 6, finding meltdown directly related to laser energy and optimal weld strength achieved through laser power and welding speed combination, while higher weld pressure increased meltdown but reduced weld strength. Amanat et al. Ref 13 investigated LTW of PEEK (polyether ether ketone) using Clearweld®, finding welding speed as the key factor influencing bond strength, and semi-crystalline PEEK exhibiting higher weld strengths than amorphous PEEK. Vidal et al. Ref 14 studied the LTW of ABS (acrylonitrile butadiene styrene), emphasizing the impact of CNT (carbon nanotube) concentration as laser-absorbing media on weld formation and mechanical properties, highlighting sensitivity to laser intensity and absorption coefficients. Mamuschkin et al. Ref 15 successfully utilized an absorber-free LTW method with pulsed 2-μm wavelength lasers, showcasing the potential for uniform seams and simplified focal position adjustments, enhancing welding efficiency. Pereira et al. Ref 16 explored LTW of polymers, particularly Nd:YAG laser welding of polyamide 6 joints, revealing the impact of laser beam diameter reduction, the efficiency of scarf joints, and the significant increase in lap joint strength with additional weld passes. Ilie et al. Ref 17 investigated the laser weldability of dissimilar polymer pairs, ABS and polyamide 11, with varying thickness and pigment compositions, using an experimental design approach, highlighting the significant influence of laser power, clamping pressure, and multiple passes on weld strength. Kumar et al. Ref 18 explored wobble LTW of dissimilar transparent polymers (acrylic/polycarbonate), emphasizing improved material intermixing, joint strength, and micromechanical joining facilitated by homogenized heat distribution and turbulence in the weld pool. Yu et al. Ref 19 employed metal particle absorbents, including magnesium zinc alloy, zinc, and tin particles, in LTW of transparent thermoplastics. Metal absorbents showed advantages with minimal thermoplastic decomposition and strong interfacial interaction, resulting in the highest shear force among the tested materials. Liu et al. Ref 20 performed LTW of PEEK and carbon fiber-reinforced PEEK (CFR-PEEK), finding that the carbon fibers in CFR-PEEK increased decomposition thresholds and joint strength due to their high thermal conductivity. LTW extends beyond polymer-to-polymer welding and can also be used for joining polymers with metals (Ref 21).

Analytical and numerical studies play a crucial role in explaining the underlying physics and mechanics of laser materials processing (Ref 22-24), with several researchers utilizing simulations to gain insights into various aspects of LTW processes. Mayboudi et al. Ref 25 developed a thermal model for LTW of polyamide 6, which, when improved to account for laser beam scattering, showed good agreement with experimental data. Acherjee Ref 26 developed a numerical model to analyze the transient temperature field in quasi-simultaneous LTW, revealing factors affecting weld zone temperature, width, and distortion. Schkutow and Frick Ref 27 investigated how wavelength-dependent absorption properties of polymers and carbon black affect temperature fields and melt pool geometry in LTW. A simulation model is employed to optimize weld properties through wavelength adaptation in the spectral range of 1.4 to 2.0 μm, potentially enhancing load-bearing capacity and gap-bridging capabilities. Lakemeyer and Schoppner Ref 28 numerically investigated the influence of energy input and welding temperature on weld quality, revealing that while both factors impact weld strength, the welding temperature exhibits a higher influence. Wang et al. Ref 29 employed thermal contact conductance to address the inaccuracy in traditional LTW models and verify it through experiments, demonstrating the significance of thermal contact conductance in the accurate finite element modeling for LTW. Prabhakaran et al. Ref 30 employed numerical simulation, utilizing a finite difference approach to investigate the impact of welding conditions on time-dependent temperature profiles during LTW of polyamide 6. Acherjee Ref 31 presented a numerical investigation into the thermal and thermomechanically induced stress field during LTW of polymers, employing a 3D transient thermomechanical model with sequential coupled field analysis and considering various thermal phenomena and viscoplastic effects. Goyal et al. Ref 32 proposed a hybrid technique, combining experiments and numerical analysis, predicting absorptivity and joint interface temperature in LTW of PC (polycarbonate) with electrolytic iron powder as an absorber.

Polypropylene (PP) is a versatile and widely used engineering material known for its excellent combination of physical, mechanical, and chemical properties. This is utilized in numerous applications, including packaging, automotive components, medical devices, construction materials, electrical appliances, agriculture, stationery, and consumer goods. Xu et al. Ref 33 investigated laser energy scattering in transparent amorphous PC and semi-crystalline PP polymers during LTW, analyzing its dependence on factors like part thickness, glass fiber content, and crystallinity, providing insights for LTW optimization. Ghasemi et al. Ref 34 investigated how various quasi-simultaneous LTW parameters affect the meltdown process in PC and PP materials. The results showed that laser power impacted induction time, while scan speed and clamping pressure influenced total meltdown. Chen et al. Ref 35 addressed the challenges posed by low laser transmittance in LTW of fiberglass-doped PP and fiberglass-doped ABS, presenting a hybrid heat source model and mathematical relationships for guiding the practical production of LTW in these materials. Nguyen et al. Ref 36 modeled the scattering behavior of PP using the four-flux model, investigated the laser beam absorption profile during LTW, and experimentally demonstrated the advantages of quasi-simultaneous irradiation in reducing heat-affected zone (HAZ) offset and vertical extent. Rohricht et al. Ref 37 investigated crystal structure in HAZs of overlapping PP welds, correlating force increase with weld seam cross-sectional area and employing thermal simulations for predictive HAZ analysis. Ali et al. Ref 38 investigated the influence of carbon black and other parameters on high-speed LTW, employing a numerical model to analyze the effects on weld characteristics, revealing successful welding with specific carbon black concentrations in isotactic polypropylene com-

posites. Dave et al. Ref 39 explored the LTW of isotactic PP and its carbon black composites, highlighting the influence of polymer crystallinity on weld integrity and optimizing carbon black content for enhanced weld quality and speed. Prior LTW studies of PP have significantly contributed to the understanding of various aspects of the process, such as laser energy scattering, welding parameters, challenges with low laser transmittance, crystal structure in heat-affected zones, and the influence of carbon black on high-speed LTW. However, there remains a notable research gap in the comprehensive analysis of LTW of PP, with a lack of focus on in-depth parametric interplay, joint quality, fracture modes, and detailed morphological characteristics. Addressing this gap, the present study aims to provide a more thorough and integrated examination of LTW of PP by systematically analyzing parametric interplay, evaluating joint quality, examining fracture modes in welded structures, and scrutinizing fracture surface characteristics and weld morphology. This paper advances the understanding of LTW of PP, providing a deeper and more comprehensive understanding of the LTW process, thereby offering valuable insights for practical applications.

2. Thermal Characterization of Polypropylene

In the LTW process, the molten polymer within the weld pool facilitates improved heat transfer between the parts, consequently enhancing the bonding strength. It is crucial to maintain the temperature during welding below the decomposition threshold while ensuring it remains significantly above the glass transition temperature (for amorphous polymers) or the melting point (for semi-crystalline polymers) to achieve high-quality welds. DSC (differential scanning calorimetry) and TGA (thermogravimetric analysis) results provide crucial data on polymer melting temperatures, crystallization behavior, thermal stability, and decomposition temperature, guiding the selection of LTW parameters and ensuring weld quality and reliability.

Non-isothermal DSC tests are conducted using a Discovery DSC 25 to analyze the thermal characteristics of natural PP and PP containing 0.2 wt.% carbon black (CB-PP). Thin films with a 200-μm thickness are prepared, and the untreated films undergo a heating–cooling–heating cycle from − 50 to 200 °C at a heating rate of 10 °C/min. The melting temperatures (T_{m2}) are determined from the melting peaks of the first and second heating scans, resulting in values of 165.68 and 161.00 °C for natural PP, and 165.71 and 161.60 °C for the CB-PP, as depicted in Fig. 1. The sudden peaks in temperature observed in Fig. 1 during the non-isothermal DSC tests are indicative of significant phase transitions occurring within the material, such as melting or crystallization. These peaks represent critical points where the material undergoes rapid changes in its thermal state, reflecting its inherent properties and structural transformations. In non-isothermal DSC tests, the material undergoes a heating–cooling–heating cycle. The temperature variance between the initial and subsequent heating scans (scan 1 and scan 2) highlights the dynamic response of the material to the thermal cycle, influenced by prior thermal history. Despite controlled conditions, the material undergoes thermal transitions during the initial heating–cooling cycle, altering its internal structure and properties. Reheating in the second scan maintains prior thermal effects, causing slight deviations in behavior and observed temperature differences, including melting points (Ref 40). The crystallization temperature (T_c) is determined as 115.19 °C for natural PP and 119.08 °C for CB-PP, while the onset temperature of crystallization is 123.48 °C for natural PP and 124.37 °C for CB-PP, with enthalpy changes of 65.92 and 104.92 J/g, respectively, calculated from cooling scan peak data. The degree of crystallinity for natural PP and CB-PP is determined by calculating the ratio of the melting enthalpy from the second heating cycle (52.186 and 78.849 J/g, respectively) to the enthalpy of fusion for the ideal PP crystal (205 J/g) (Ref 41). The degree of crystallinity is found to be 25.21% in the natural PP and 38.09% in the CB-PP. The addition of carbon black pigments to the PP matrix alters the polymer chain segment mobility, affecting crystallization by acting as nucleating agents and reducing nucleation barrier energy, thus increasing crystallinity during heterogeneous crystallization (Ref 42).

The thermal stability of natural PP and CB-PP is assessed using TGA (Discovery SDT 650). TGA measures mass/weight changes and their rates with temperature, time, and atmosphere. Figure 2 illustrates the weight loss curves for PP and CB-PP, revealing the decomposition onset temperature and peak temperature for assessing thermal stability. The decomposition onset temperature of natural PP is 278.48 °C, but in the presence of carbon black, it notably increases by about 22.31 °C (reaching 300.79 °C) at 0.2 wt.% concentration. The decomposition peak temperatures for natural PP and CB-PP are 404.87 and 412.80 °C, respectively, with analysis durations of 46.35 and 51.05 minutes to decompose 98.21% of natural PP and 97.15% of CB-PP, respectively. The higher decomposition temperature in CB-PP indicates that carbon black enhances its thermal stability, making it more resistant to decomposition. Analysis durations in TGA serve as a critical metric for understanding material decomposition kinetics. Notably, with durations of 46.35 minutes for natural PP and 51.05 minutes for CB-PP, the measured difference suggests a slower decomposition rate in CB-PP (97.15%) compared to natural PP (98.21%). This highlights the impact of carbon black, influencing not only the decomposition temperature but also the kinetics of the decomposition process. Carbon black enhances polymer thermal stability by absorbing and dispersing heat energy, delaying decomposition. It also reinforces the polymer matrix, increasing resistance to degradation. Hence, CB-PP exhibits improved thermal stability over natural PP, evident in its higher decomposition temperature and slightly longer decomposition duration. This information is vital for comprehending the thermal stability and decomposition behavior of polymers, which is crucial in diverse applications, including welding processes. In Fig. 2, the DTG (derivative thermogravimetry) plot is presented alongside the TGA plot. In the DTG plot, the first and second minor heat flow peaks are endothermic, indicating bond breaking in PP before degradation initiates (Ref 43), while the major peaks represent the final degradation (Ref 44), including the melting transition of natural PP and CB-PP, marking the temperature at which complete degradation occurs.

3. Laser Transmission Welding of Polypropylene

A CNC (computer numerical control) fiber laser welding system, depicted in Fig. 3(a), is utilized for LTW of polypropylene. This laser system comprises an IPG Photonics 1-kW fiber

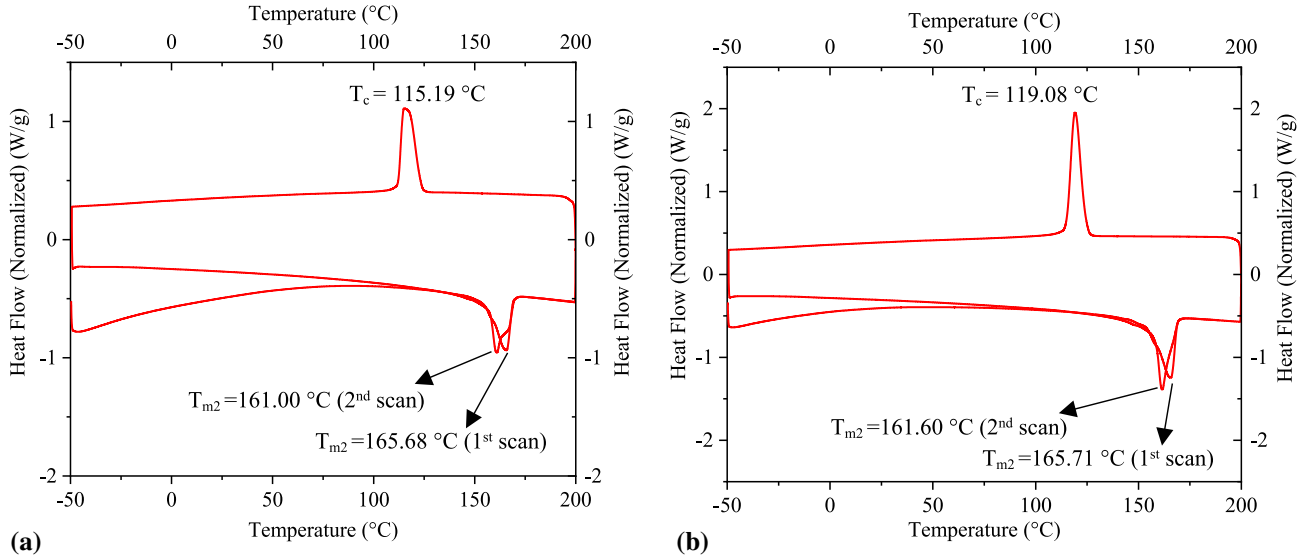

Fig. 1 DSC curves of (a) polypropylene and (b) polypropylene containing 0.2 wt. % carbon black

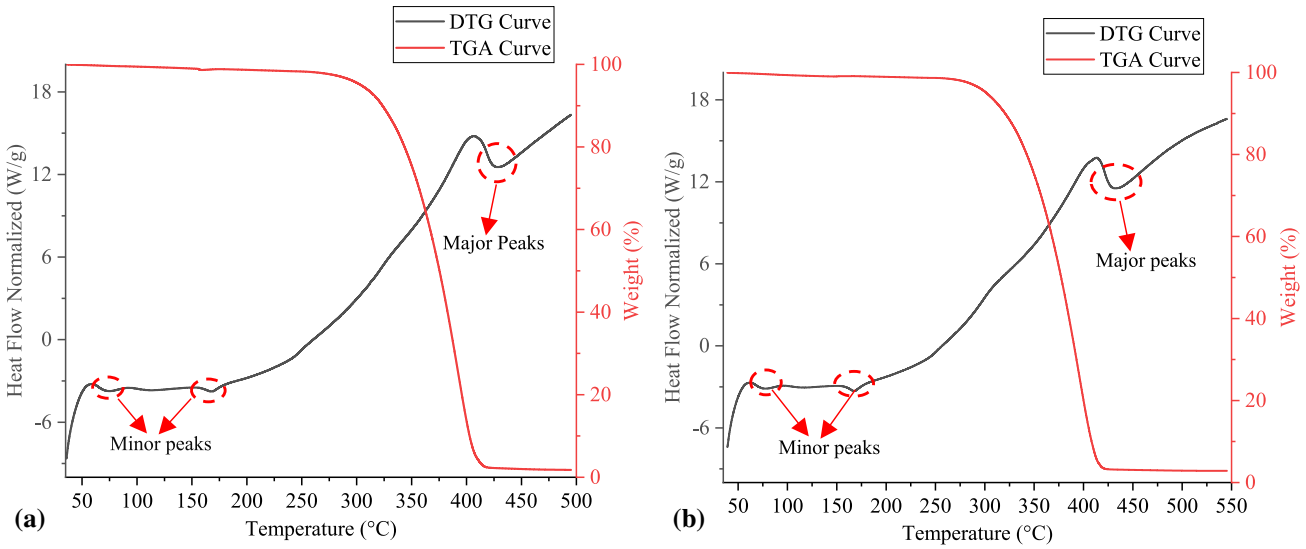

Fig. 2 TGA and DTG curves of (a) polypropylene and (b) polypropylene containing 0.2 wt. % carbon black

laser source operating at 1070 ± 10 nm wavelength, a welding head with a CCTV viewing camera, a 3-axis servo drive motion system for CNC table and laser head movement, a shielding gas supply system, and a chiller unit. Additionally, a clamping device is employed to securely hold the PP specimens during welding, ensuring intimate contact between mating surfaces and applying sufficient clamping pressure. The laser optic has a focal length of 150 mm, and the defocused section of the laser beam is employed during LTW (Fig. 3b) to achieve uniform heat distribution and an appropriate energy density for polymer welding. The camera attached to the laser welding head and the laser beam converge at a common spot, establishing a reference point for the focal point of the laser beam. The defocus distance is then measured from this point using the z-axis value displayed on the HMI (human–machine interface) screen. Alternatively, the measurement can be obtained through the scale integrated with the z-axis CNC drive unit. Laser power, scanning speed, and defocus distance are systematically adjusted to different levels, controlling the heat input and interaction time during the LTW process. These parameters influence melting and fusion at the weld interface, consequently impacting the weld quality, assessed through parameters like weld strength and weld seam dimensions. Table 1 displays the process parameters and their respective ranges employed in the experiments. These parameter ranges are determined through a series of preliminary experiments, ensuring criteria such as the smooth appearance of the weld seam and the absence of visible defects are met. In this research, a fractional factorial design is employed, wherein a full factorial combination of two factors is executed while maintaining the third factor at its midvalue. This strategic approach aimed to optimize the experimental design by reducing the number of runs while retaining the essential information regarding the main effects and interactions of the factors. This allowed for a more efficient allocation of resources while ensuring a comprehensive understanding of the impact of experimental variables on the studied outcomes. This results in

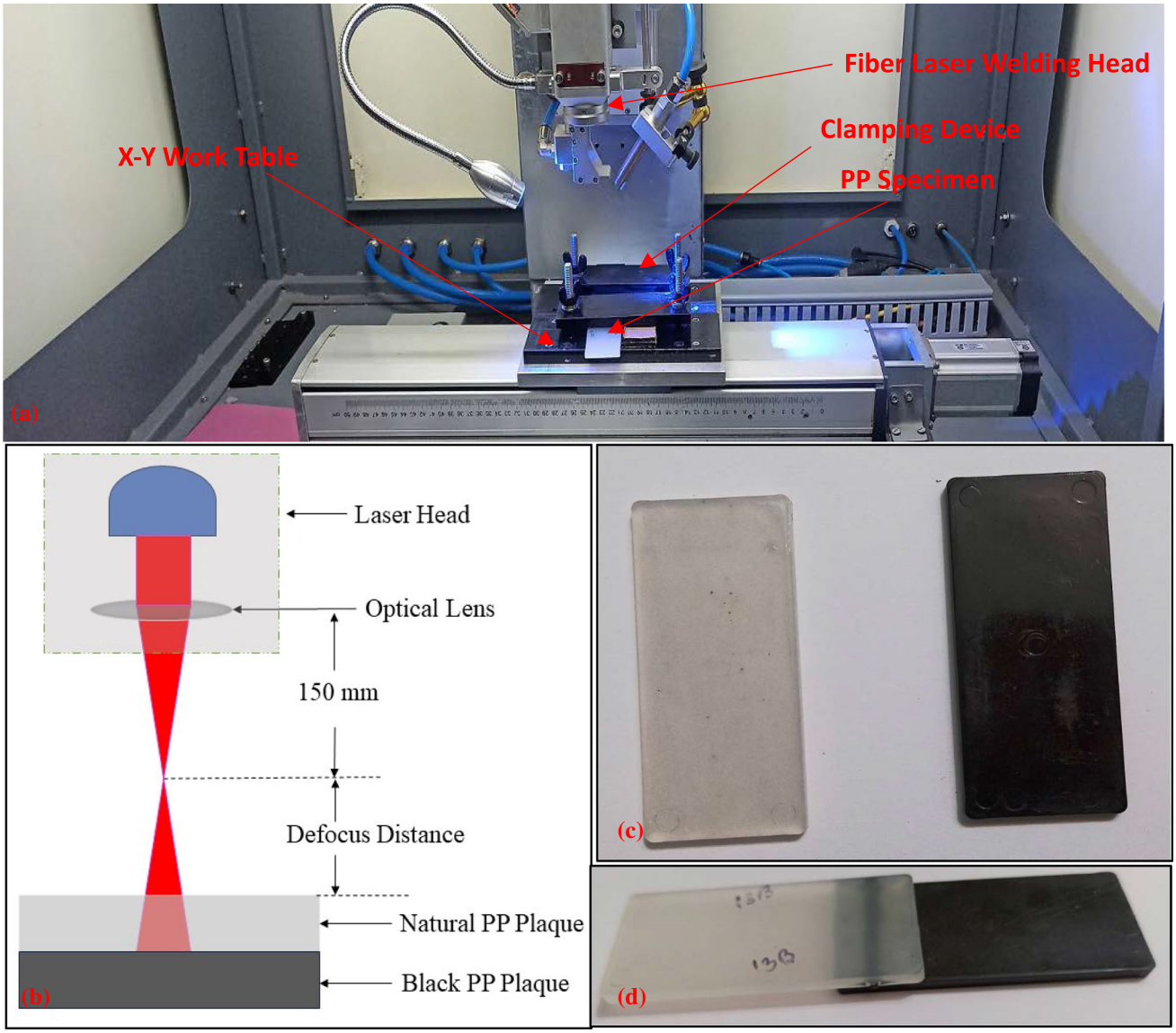

Fig. 3 (a) Image of the experimental setup, (b) schematic representation of the LTW process, (c) injection-molded natural and black PP workpieces, and (d) laser-welded PP sample

Table 1 Process parameters and their ranges

Process parameters	Units	Ranges	Levels				
			1	2	3	4	5
P: Laser power	W	100-300	100	150	200	250	300
S: Scanning speed	mm/s	60-120	60	75	90	105	120
F: Defocus distance	mm	50-70	50	55	60	65	70

a reduction of experimental runs to 75 in a fractional factorial design, compared to 125 runs in a standard full factorial design. The experimental layout for investigating the impact of independently controllable process parameters is illustrated in Table 2.

Natural and black PP plaques are employed as work materials. PP is a versatile engineering material known for its outstanding chemical resistance, mechanical properties, and ease of processing, making it suitable for diverse applications. Natural PP has a translucent or whitish appearance, resulting in a significant degree of laser light transmittance. However, in scenarios where laser absorption is required, such as in LTW processes, modifications to the PP material are necessary to enhance its absorptive properties. The black PP is produced by blending natural PP granules with 0.2% carbon black by weight, whereas the natural PP plaques are directly produced from natural PP granules. Carbon black is chosen for its strong light-absorbing characteristics across a wide spectrum of wavelengths, including those emitted by laser sources (Ref 3). Incorporating carbon black into the PP matrix enhances its laser energy absorption, making it ideal for the LTW process (Ref 38). These PP plaques are injection molded into dimensions of 80 mm × 35 mm × 4 mm each (Fig. 3c), using a custom-made mold. Prior to welding, the natural PP is positioned over the black PP on a welding fixture with a 20 mm × 35 mm overlap and securely clamped in place. The CNC-Z axis is then used to adjust the position of the laser head

Table 2 Experimental plan and measured response values

	Process parameters			Weld strength, N/mm			Weld width, mm		
					Deviations			Deviations	
Exp. No.	P, W	S, mm/s	F, mm	Mean value	Absolute	%	Mean value	Absolute	%
1	100	60	60	35.78	1.50	4.20	2.75	0.08	3.00
2	150	60	60	46.83	2.48	5.30	2.99	0.06	2.10
3	200	60	60	53.86	3.82	7.10	3.20	0.07	2.30
4	250	60	60	56.88	1.19	2.10	3.38	0.17	5.00
5	300	60	60	55.88	6.25	11.18	3.53	0.22	6.20
6	100	75	60	41.87	2.55	6.10	2.66	0.06	2.30
7	150	75	60	52.39	2.15	4.10	2.90	0.09	3.20
8	200	75	60	59.90	1.86	3.10	3.10	0.10	3.30
9	250	75	60	61.40	3.13	5.10	3.27	0.13	4.10
10	300	75	60	59.88	3.65	6.10	3.41	0.13	3.70
11	100	90	60	43.74	0.87	2.00	2.59	0.06	2.40
12	150	90	60	53.75	2.80	5.20	2.81	0.10	3.40
13	200	90	60	59.74	2.51	4.20	3.00	0.08	2.70
14	250	90	60	61.72	2.30	3.72	3.16	0.07	2.20
15	300	90	60	59.69	2.46	4.12	3.30	0.14	4.30
16	100	105	60	41.41	2.07	5.00	2.52	0.06	2.30
17	150	105	60	50.90	3.82	7.50	2.73	0.10	3.50
18	200	105	60	56.38	4.79	8.50	2.91	0.12	4.10
19	250	105	60	57.84	3.18	5.50	3.07	0.11	3.60
20	300	105	60	55.28	3.87	7.00	3.19	0.14	4.40
21	100	120	60	34.87	1.57	4.50	2.46	0.04	1.80
22	150	120	60	43.85	1.53	3.50	2.66	0.11	4.30
23	200	120	60	48.80	3.17	6.50	2.83	0.09	3.30
24	250	120	60	49.74	3.23	6.50	2.97	0.10	3.50
25	300	120	60	46.67	4.90	10.50	3.09	0.20	6.40
26	100	90	50	34.75	1.29	3.70	2.28	0.02	0.90
27	150	90	50	43.06	1.51	3.50	2.42	0.05	2.10
28	200	90	50	47.35	1.33	2.80	2.54	0.07	2.90
29	250	90	50	47.63	1.48	3.10	2.62	0.08	2.90
30	300	90	50	43.90	0.48	1.10	2.68	0.19	7.20
31	100	90	55	40.83	1.84	4.50	2.47	0.06	2.60
32	150	90	55	49.99	2.05	4.10	2.66	0.07	2.70
33	200	90	55	55.13	2.04	3.70	2.81	0.10	3.40
34	250	90	55	56.26	1.91	3.40	2.93	0.07	2.30
35	300	90	55	53.38	3.36	6.30	3.03	0.21	6.80
36	100	90	60	43.74	1.68	3.83	2.59	0.09	3.50
37	150	90	60	53.75	1.45	2.70	2.81	0.06	2.20
38	200	90	60	59.76	2.57	4.31	2.96	0.09	3.01
39	250	90	60	61.72	1.67	2.70	3.16	0.17	5.30
40	300	90	60	59.69	2.27	3.80	3.30	0.21	6.30
41	100	90	65	43.48	2.74	6.30	2.63	0.10	3.70
42	150	90	65	54.34	1.58	2.90	2.89	0.03	1.20
43	200	90	65	61.19	2.39	3.90	3.12	0.07	2.40
44	250	90	65	64.01	1.54	2.40	3.32	0.17	5.10
45	300	90	65	62.83	2.83	4.50	3.50	0.13	3.70
46	100	90	70	40.06	4.42	11.02	2.60	0.13	4.90
47	150	90	70	51.77	1.19	2.30	2.89	0.05	1.90
48	200	90	70	59.46	2.08	3.50	3.16	0.07	2.30
49	250	90	70	61.14	0.79	1.30	3.40	0.22	6.50
50	300	90	70	62.80	2.32	3.70	3.61	0.17	4.70
51	200	60	50	33.88	2.74	8.10	2.63	0.11	4.30
52	200	75	50	42.72	3.12	7.30	2.58	0.10	3.70
53	200	90	50	47.35	2.51	5.30	2.54	0.10	3.80
54	200	105	50	47.78	1.72	3.60	2.50	0.07	2.70
55	200	120	50	44.00	1.41	3.20	2.47	0.08	3.10
56	200	60	55	45.46	1.95	4.30	2.96	0.07	2.40
57	200	75	55	52.40	2.41	4.60	2.88	0.08	2.70
58	200	90	55	55.13	1.93	3.50	2.81	0.05	1.90
59	200	105	55	53.66	1.72	3.20	2.74	0.06	2.30
60	200	120	55	47.98	1.82	3.80	2.69	0.03	1.10

Table 2 continued

Exp. No.	Process parameters			Weld strength, N/mm			Weld width, mm		
	P, W	S, mm/s	F, mm	Mean value	Deviations		Mean value	Deviations	
					Absolute	%		Absolute	%
61	200	60	60	53.86	1.67	3.10	3.20	0.08	2.60
62	200	75	60	58.91	1.59	2.70	3.10	0.07	2.10
63	200	90	60	59.83	1.43	2.40	2.97	0.08	2.79
64	200	105	60	56.38	1.64	2.90	2.92	0.11	3.90
65	200	120	60	48.80	0.63	1.30	2.83	0.05	1.70
66	200	60	65	59.10	1.12	1.90	3.37	0.10	2.90
67	200	75	65	62.24	1.43	2.30	3.24	0.07	2.30
68	200	90	65	61.19	1.47	2.40	3.12	0.12	3.70
69	200	105	65	55.92	1.06	1.90	3.00	0.09	3.00
70	200	120	65	46.45	2.04	4.40	2.90	0.09	3.00
71	200	60	70	61.16	2.87	4.70	3.45	0.11	3.10
72	200	75	70	62.41	2.62	4.20	3.30	0.08	2.30
73	200	90	70	59.46	3.63	6.10	3.16	0.17	5.30
74	200	105	70	52.30	3.82	7.30	3.02	0.17	5.50
75	200	120	70	40.93	5.30	12.95	2.89	0.21	7.40

to set a specific defocus distance. Laser power and scanning speed are configured through human–machine interface software, and the laser beam is precisely targeted at the centerline of the overlapping area of the plaques. The laser irradiation induces melting at the interface of the polymers, and once solidified, the welded samples are removed from the fixture. The resulting weld specimen is shown in Fig. 3(d).

4. Assessment of Weld Strength and Weld Seam

A universal testing machine (Tinius Olsen: Model 5ST) is employed for the weld strength testing of the welded specimens (Fig. 4a). Adjustments are made to prepare the specimens for shear testing, which includes attaching two plastic plaques to the gripping area, as depicted in Fig. 4(b), to minimize bending moments at the weld line. Subsequently, roughening is done at both ends of each specimen at the gripping area to prevent slippage during the lap-shear test. The shear-lap joints are tested under ambient temperature conditions, maintaining a constant crosshead speed of 0.5 mm/min. Polymers exhibit time-dependent viscoelastic behavior (Ref 31). A slower crosshead speed in tensile testing ensures a controlled force application, allowing the material adequate time to respond without abrupt changes. This is crucial for capturing accurate mechanical properties. Slower speeds also reduce strain rate sensitivity impact, and various studies employed 0.5 mm/min (Ref 45, 46) or 1 mm/min (Ref 47) for tensile testing of polymer welds. The maximum load (N) at which the welded specimen fails is recorded (Fig. 4c). Weld strength is assessed as the maximum load to failure per unit length of the weld (N/mm). Two distinct failure modes are evident in the shear-tested specimens, as shown in Fig. 4(d): shear failure occurring at the joint interface, and base polymer fracture near the weld line (Ref 14). Specimens with higher weld strengths mainly exhibit fractures near the end of the weld seam in the base polymer. This indicates that the weld is stronger than the adjacent base PP near the weld seam, which has been affected by heat but not to the point of melting in the heat-affected zone. Furthermore, it is noteworthy that in all instances, only the black PP fractures, not the natural PP. This results from the direct laser irradiation and heating experienced by the black PP, which, due to its much higher absorption of the laser beam compared to natural PP, absorbs a substantial amount of laser energy. As a result, it undergoes more significant heating and heat-induced changes in mechanical strength. In contrast, natural PP is less affected by heat because it undergoes indirect heating, relying on heat conduction from the black PP through contact. Consequently, in cases where the failure occurred due to fractures in the base polymer, it consistently resulted in fractures occurring in the black PP near the weld seam. Samples sheared from the weld interface exhibit relatively weaker weld strength, which is a consequence of the relatively weaker bonding. This may be attributed to lower heat input or a shorter interaction time with the laser irradiation due to the selected parameter settings. It has been observed that partial decomposition at the weld zone (Fig. 5), located in the centerline of the weld seam, resulting from the Gaussian laser intensity distribution, does not undermine the weld strength. This occurrence is linked to higher heat input, which simultaneously widens the weld width and provides a larger area to withstand shear forces. Hence, shear failure at the weld interface is observed in cases where incomplete fusion or partial/shallow melting occurs at the weld interface. Conversely, fracture occurred in the base PP near the weld line when adequate bonding and/or a wide weld seam have been achieved due to optimal heating and melting. This includes scenarios where partial decomposition occurred at the centerline of the weld seam, resulting in a wider weld seam. Importantly, within the studied parameter range, which encompassed numerous trials, no substantial polymer decomposition is observed.

Weld width measurements for each specimen are performed using an Olympus SZ61 stereo microscope equipped with a camera mount (Fig. 5a). Microscope eyepieces are aligned along the weld width, and magnification is adjusted to visualize the weld boundaries. Subsequently, Olympus LCmicro image analysis software is utilized to measure the weld width at three distinct locations, with the resulting values averaged to obtain the average weld width (Fig. 5b). The weld width is determined through the top translucent plaque (Fig. 5c), which is the apparent weld width. This measurement's validity is confirmed

by measuring the weld width at the weld interface by removing the top plaque in a few samples (Fig. 5d), and it is found to be consistent and nearly equal. As a result, the weld width dimension is consistently measured through the top translucent plaque. As evident in Fig. 5(d), there are substantial traces of natural PP residue over the black PP at the weld interface following the removal of the top natural PP layer, indicating excellent bonding at the weld interface. Furthermore, this figure reveals partial decomposition of the black PP along the centerline of the weld seam, creating a thin channel in the middle. However, the strong bonding in the surrounding materials, indicated by the significant presence of natural PP residue over the black PP, contributes to the strength of the weld.

5. Effect of Parametric Interactions on Weld Strength and Width

Table 2 furnishes both the experimental plan and the measured values of responses of interest, providing insight into the investigation of the impact of independently controllable process parameters on the responses. At least three weld samples are employed per experimental run to ensure result consistency. The average of the observed results from these three samples is used for parametric analysis. If the deviation among repeated samples exceeds 10% in certain cases (as shown in Table 2, Exp. No. 5, 25, 46, 75), the sample size is increased to four or more to ensure result reliability. Table 2 displays the mean values and deviations from repeat experiments.

It is observed that the maximum strength achieved through the selected parameters in this study for the weld is 59.58% of the base material (natural PP). The breaking loads of natural PP and black PP, with samples 35 mm wide and 4 mm thick as the workpiece, are 3760 and 3900 N, respectively. The maximum breaking load of the weld achieved is 2240.35 N, normalized over a 35-mm-long weld line (width of the sample), resulting in 64.01 N/mm as shown in Table 2 (Exp. No. 44). The comparison is based on breaking load because the base plate undergoes tensile testing, while the welded samples undergo lap-shear testing; the base fails due to tension, whereas the weld may fail due to shear, tension, or both, possibly leading to different planes of failure. Therefore, the comparision of strength between the base material and the weld sample is made in terms of load-bearing capacity (N). It is worth noting

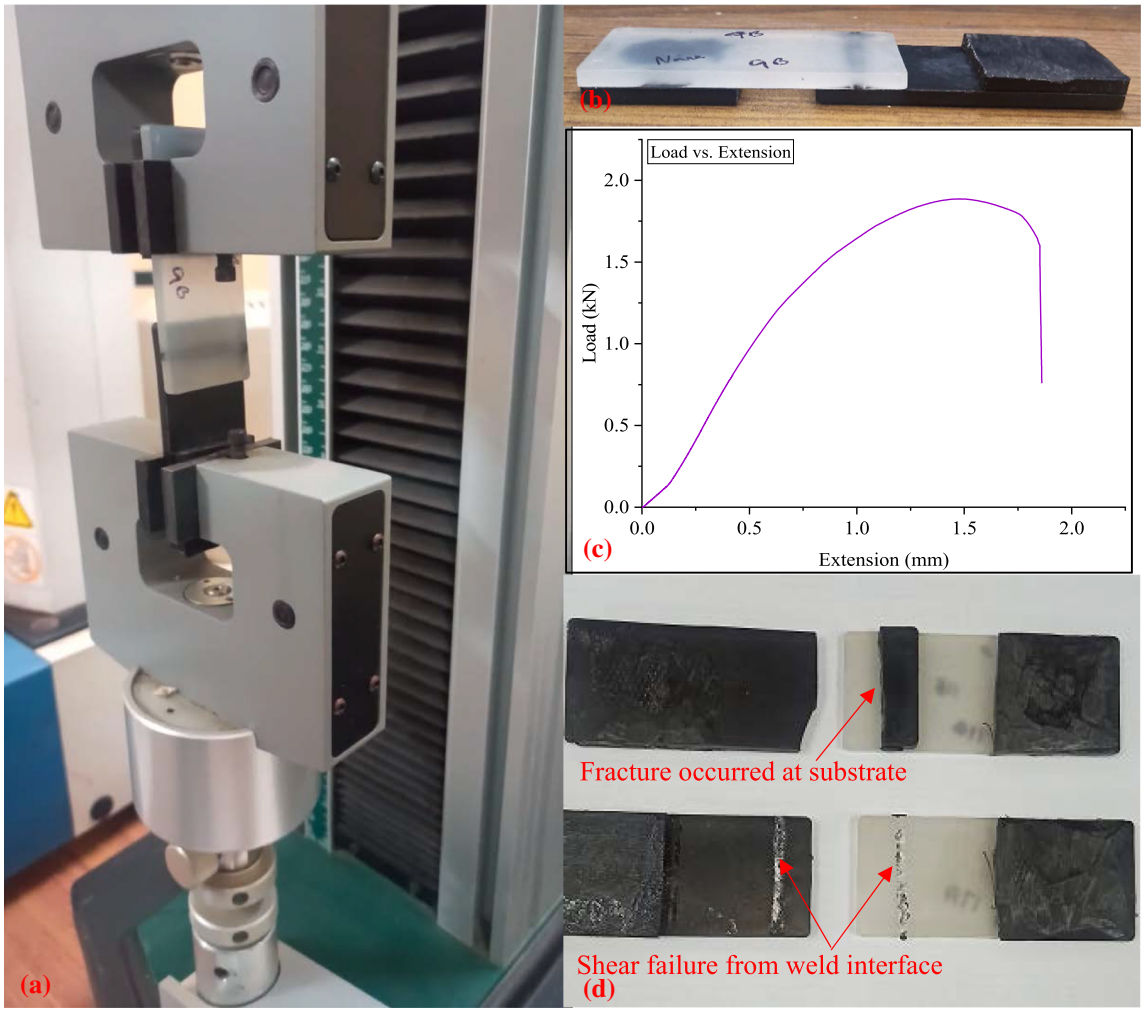

Fig. 4 (a) Photograph of the weld strength testing apparatus, (b) prepared specimen for lap-shear tests, (c) load–extension plot of a weld sample during lap-shear tests, and (d) fractured weld samples.

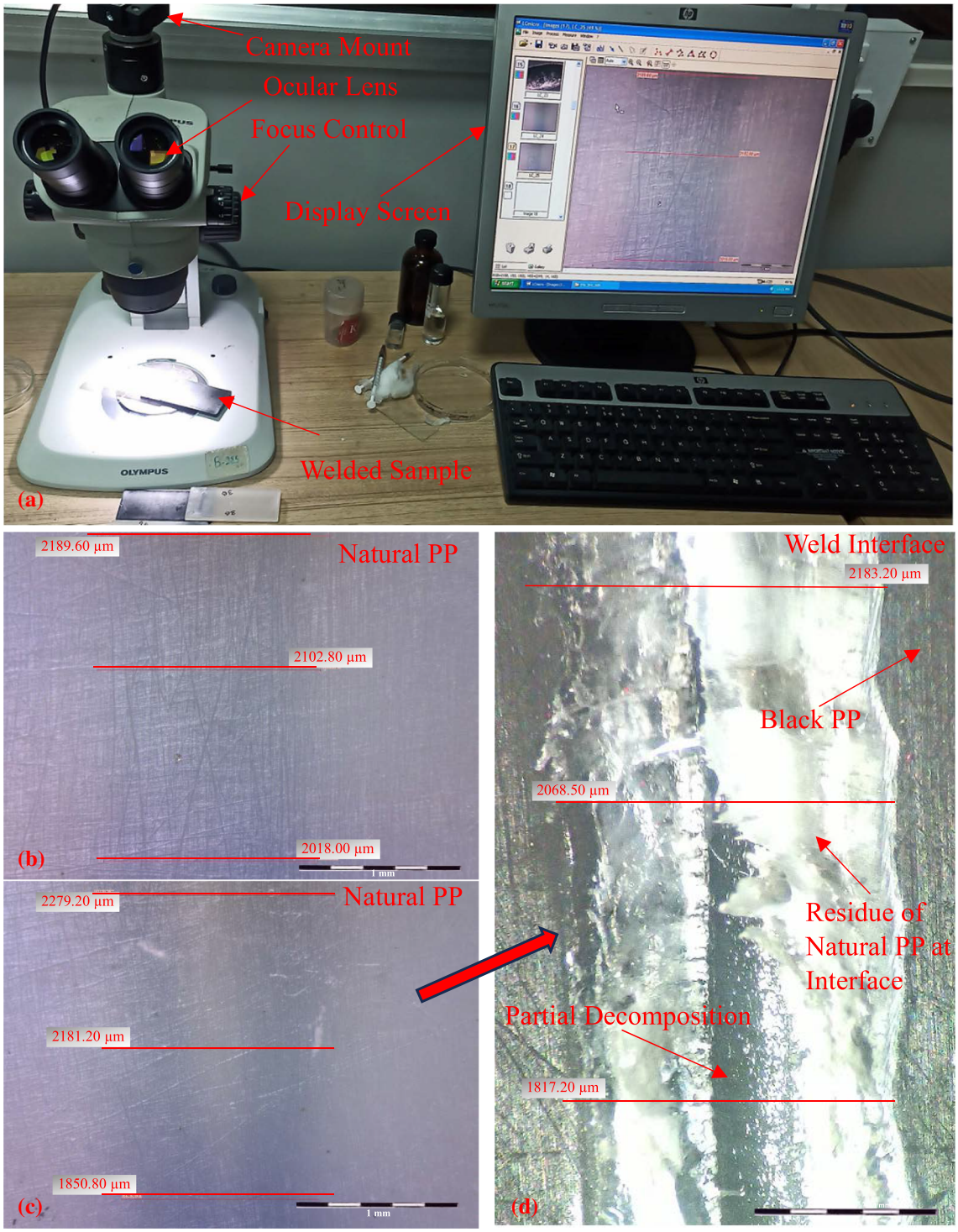

Fig. 5 (a) Photograph of the weld width measuring apparatus, (b, c) measured weld width through the top natural PP, and (d) measured weld width at the weld interface after removing the top natural PP.

that the strength ratio of the weld to the base material may further improve with optimized process conditions.

Figure 6(a) and (b) maps the experimentally explored parameter space through cube plots, visually presenting response means across various combinations of factor levels. These plots not only furnish parameter ranges but also offer insights into the process responses pertinent to the study, weld strength (Fig. 6a) and weld width (Fig. 6b). Each cube plot explains the relationship between three selected welding parameters and a specific response at the design space boundary points. Purposefully highlighting weld strength and width responses at this boundary enriches the visual representations

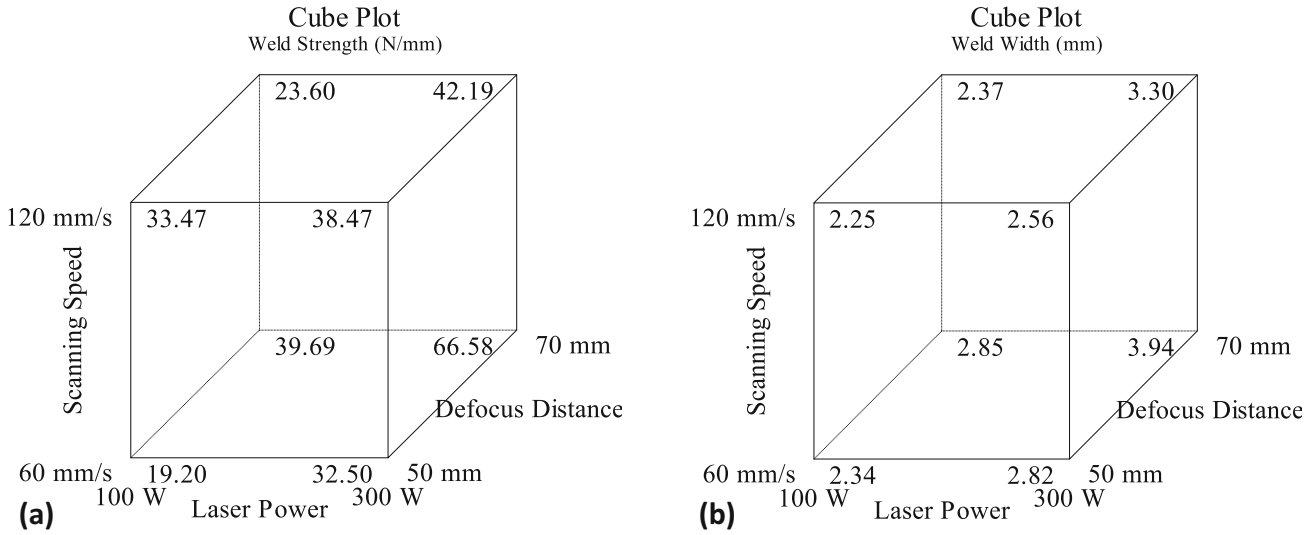

Fig. 6 (a, b) Process parameters and their corresponding ranges used in the experiments

and affords a holistic overview of attained response values within carefully defined experimental conditions. However, the following paragraphs will provide a comprehensive analysis of how process responses are influenced by LTW parameters and their interactions.

It is observed from Fig. 7(a) that weld strength initially increases with laser power and then declines beyond a certain threshold. Enhanced heat generation, energy absorption, and fusion occur with increased laser power in LTW. Higher temperatures promote greater mobility of polymer chains, facilitating improved interdiffusion and entanglement across the weld interface, leading to a stronger molecular bond. However, exceeding the optimal laser power range for LTW of PP results in negative consequences such as thermal degradation, localized overheating, and potentially weaker welds due to defect formation (Ref 48). The trends observed in the experimental data reveal that, across various scanning speeds, an initial increase in laser power leads to enhanced weld strength up to a specific threshold. The inherent susceptibility of polymers to thermal degradation, coupled with their lower thermal conductivity compared to metals, emphasizes the importance of precisely controlling heat input during welding. Achieving an optimal balance between laser power and scanning speed emerges as a pivotal factor in maximizing weld strength while mitigating the risk of material degradation. This delicate equilibrium ensures effective fusion without subjecting the polymer to excessive heat-induced damage (Ref 49). Lower scanning speeds have a threshold beyond which excessive heat can lead to degradation and reduced weld strength. Conversely, higher scanning speeds enable more efficient heat dissipation, enabling increased laser power to influence weld strength positively. Within the studied parameter range, the combination of 250 W laser power and 90 mm/s scanning speed yields the highest weld strength when maintaining a constant defocus distance of 60 mm. From Fig. 7(b), it is evident that increasing laser power has the effect of widening the weld width. Laser power is directly linked to the energy supplied by the laser beam to the polymer material. Consequently, increasing laser power delivers more energy to the polymer materials being joined, leading to a greater softening of the polymers and improved weld dimensions and fusion. Furthermore, it is observed that the weld width increases as the scanning speed decreases. Reducing the scanning speed prolongs the interaction time between the laser and the polymer, resulting in a higher heat application to the polymer material. The interaction between laser power and scanning speed in LTW demonstrates that higher laser power (300 W) combined with lower scanning speed (60 mm/s) tends to result in a wider weld width.

As depicted in Fig. 7(c), it becomes apparent that the relationship between welding speed and weld strength is not linear. There exists an optimal range of welding speeds where the weld strength is maximized. Within this range, the polymer material is exposed to the right amount of heat (controlled through the exposure time) for proper melting and fusion, without the risk of excessive heat causing polymer degradation or weakening the weld. The interplay between scanning speed and defocus distance reveals a complex relationship, as evident in this figure. The reduced defocus distance concentrates the energy from the laser onto a smaller area, leading to more localized heating. In this context, employing a higher scanning speed proves effective because it minimizes the interaction time, thereby preventing excessive heating that could lead to polymer degradation or defects. Consequently, at lower defocus distances, a higher scanning speed proves beneficial in achieving superior weld strength, due to the concentrated heating and controlled exposure it provides. Conversely, at higher defocus distances, a lower scanning speed becomes essential to compensate for the reduced energy density. This ensures that the polymer material has sufficient time to absorb the necessary heat for proper melting and fusion. Defocus distance, scanning speed, and LTW weld strength are intricately linked through energy concentration, heat distribution, and achieving polymer fusion without degradation in a complex interplay (Ref 50). In the examined parameter range, the highest weld strength is achieved using a combination of 75 mm/s scanning speed and 70 mm defocus distance while keeping the laser power constant at 200 W. Figure 7(d) illustrates that higher welding speed decreases weld width, whereas increasing the defocus distance leads to an expansion of the weld width. Elevated scanning speeds decrease exposure time, yielding narrower welds. In contrast, increasing the defocus distance widens the laser beam profile on the polymer

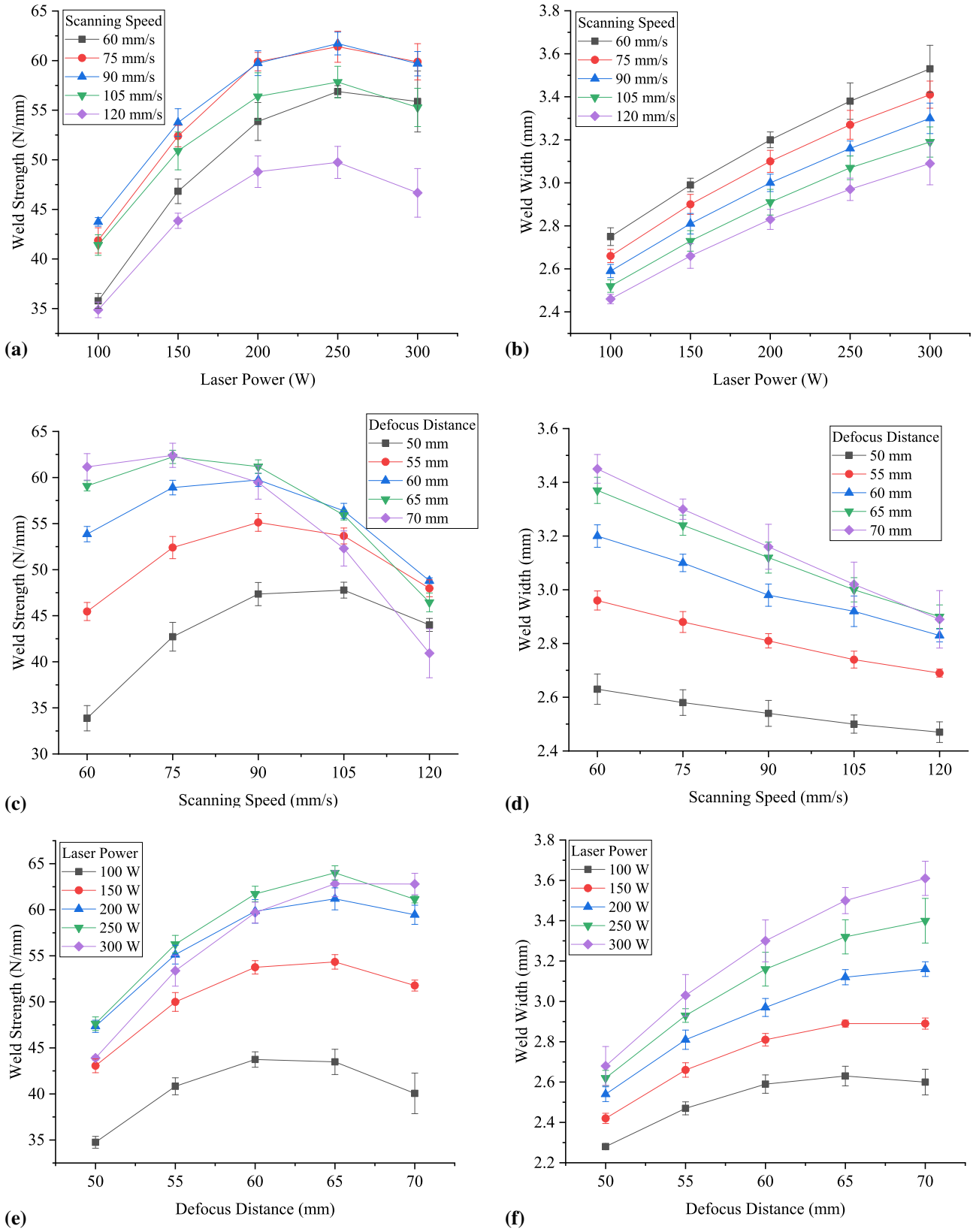

Fig. 7 Effects of laser power on (a) weld strength and (b) weld width under different scanning speeds; effects of scanning speed on (c) weld strength and (d) weld width under different defocus distances; and effect of defocus distance on (e) weld strength and (f) weld width under different laser powers

interface, resulting in broader welds. The interaction plot demonstrates that maximum weld strength is achieved when employing a low scanning speed (60 mm/s) and a high defocus distance (70 mm). Low scanning speed allows for controlled and thorough melting, while high defocus distance increases the heat-affected area. Together, these factors facilitate optimal heat absorption and molecular bonding, resulting in maximum weld strength.

As observed in Fig. 7(e), increasing the defocus distance enhances weld strength up to a certain threshold value, after which it begins to decrease. Initially, increasing the defocus distance improves energy distribution and widens the fusion zone, resulting in higher weld strength. However, beyond a specific threshold, increasing defocus distance leads to issues like reduced energy density and inefficient bonding, ultimately reducing weld strength. Figure 7(e) provides insight into the interplay of defocus distance and laser power. For low and moderate defocus distances studied, an initial augmentation in laser power correlates with an improvement in weld strength, but this trend eventually reverses. At these defocus distances, higher laser power initially augments heat input, polymer melting, and bonding efficiency. However, the tipping point is reached when excessive power leads to problems such as overheating and material damage, resulting in a decline in weld strength. In contrast, for higher defocus distances, the relationship between increasing laser power and enhanced weld strength remains consistent. This is attributed to the fact that higher power compensates for the laser beam diffusion caused by the greater defocus distance (Ref 51). This compensatory effect ensures sufficient energy delivery to the polymer, facilitating effective melting, material flow, and bonding, ultimately leading to higher weld strength. The interplay between laser power and defocus distance in LTW influences factors such as heat input and heat distribution during welding. Properly managing these factors is crucial for producing robust welds while mitigating issues such as overheating or insufficient fusion. Within the explored parameter range, the highest weld strength is achieved by combining a defocus distance of 65 mm with a laser power of 250 W, while maintaining a constant scanning speed of 90 mm/s. Figure 7(f) demonstrates that raising the defocus distance alongside laser power increases the weld width. The broader beam profile, caused by the increased defocus distance, covers a larger portion of the polymer surface, exposing more material to the laser's energy. Simultaneously, higher laser power efficiently heats this expanded area, enabling thorough polymer melting across a wider region. Consequently, a broader fusion zone and wider weld seam are achieved. The interaction plot conclusively shows that, within the range of parameters studied, the highest weld width is achieved with a combination of a high defocus distance (70 mm) and a high laser power (300 W).

Line energy, a crucial parameter in LTW, represents the energy delivered per unit length of the weld line. It necessitates a delicate balance of laser power, welding speed, and beam spot size adjustment. Typically expressed as joules per millimeter (J/mm), it quantifies the laser power-to-scanning speed ratio. Line energy serves as a dependent variable, depending upon the values of independently controllable parameters like laser power and scanning speed. Different line energy values are obtained through the division of distinct laser power levels by varying levels of scanning speed. Subsequently, the resulting values of weld strength and weld width are extracted from Table 2 for analysis purposes, focusing on the mean values of these responses. In Fig. 8(a), the weld strength in PP is depicted, showing an initial rise with line energy (up to 3 J/mm) followed by a decline. The initial strength increase is attributed to enhanced fusion, while subsequent deterioration results from substrate thermal degradation and vaporization effects. Precise line energy control is essential to ensure robust welds while averting issues like polymer thermal degradation (Ref 48). The line energy plot at each laser power level reveals a threshold value for each laser power, where weld strength increases until reaching the threshold, after which it declines. This plot depicts the sensitivity of weld strength to laser power for different line energy. Maximum weld strength is achieved at 3 J/mm line energy with a 250-W laser power. Notably, in LTW, attaining the same line energy is possible through various power and scanning speed combinations (Ref 14). As depicted in Fig. 8(a), higher laser powers (up to 250 W) coupled with faster scanning speeds produce stronger welds under the same line energy. This is primarily due to the higher power providing more energy and facilitating greater scanning speed, elevating welding temperature, and ensuring

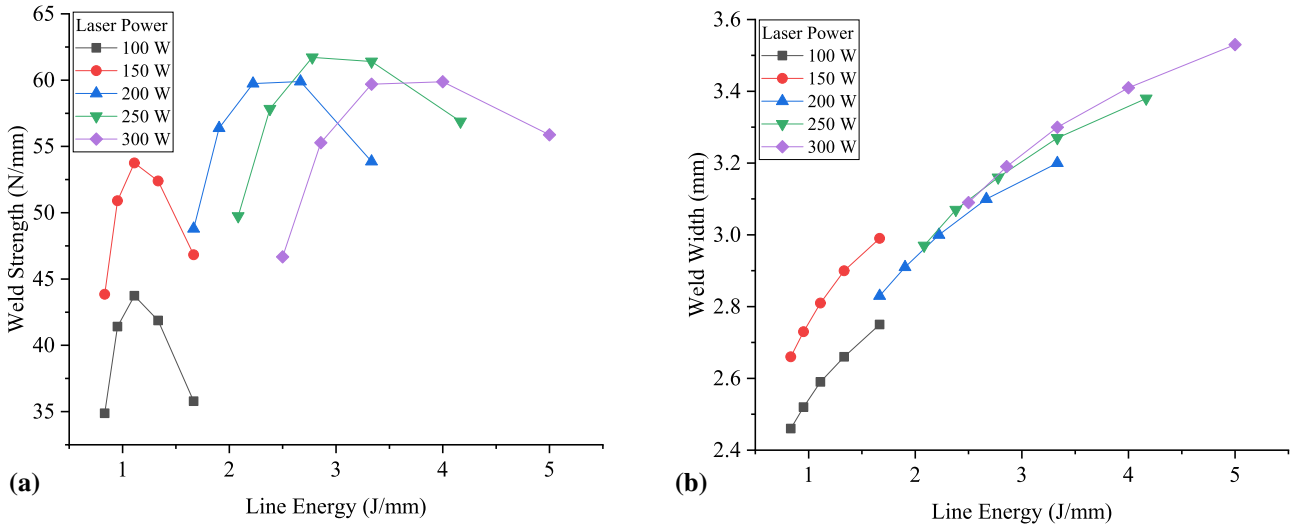

Fig. 8 Effects of line energy on (a) weld strength and (b) weld width with varying laser powers

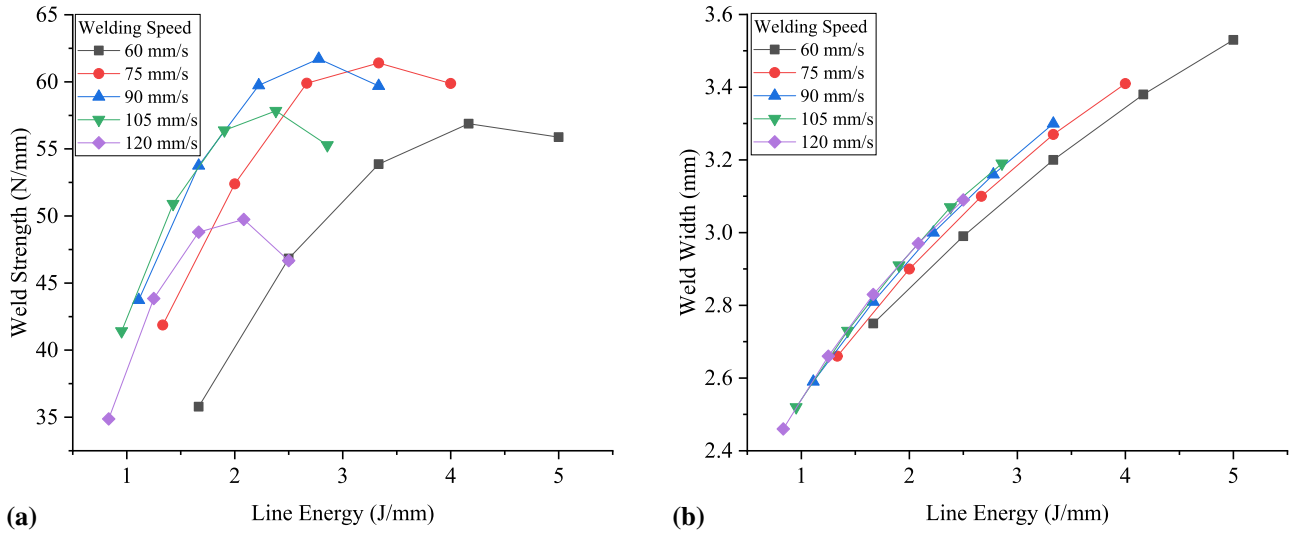

Fig. 9 Effects of line energy on (a) weld strength and (b) weld width with varying scanning speeds

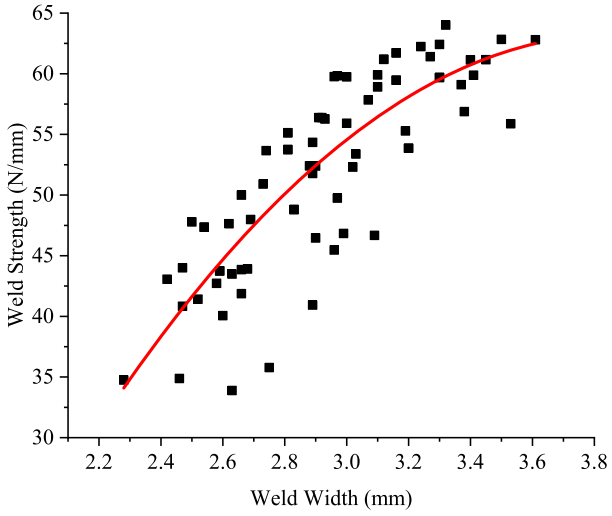

Fig. 10 Scatter plot of weld width vs. weld strength with a trendline illustrating their correlation

superior polymer surface melting and bonding. Factors such as deeper penetration, quicker heating/cooling cycles, and enhanced fusion at the welding interface all contribute to stronger joints. Conversely, lower power and slower speeds yield relatively weaker welds due to lateral energy dissipation and slow heating cycles. Figure 8(b) illustrates that higher line energy results in an increased weld width, regardless of laser power levels. This effect arises because elevated line energy concentrates more energy per unit length along the weld line, leading to increased material melting and an expanded melting zone, thereby contributing to the wider weld (Ref 52). Furthermore, it is apparent that for constant line energy, increasing laser power yields wider welds. Lower welding speeds with lower laser power emphasize heat transfer and conduction losses, particularly at slow speeds. Conversely, higher speeds with more laser power minimize heat loss, maximizing energy deposition for wider welds. Figure 9(a) shows the scanning speed sensitivity of the weld strength for different line energies. For each scanning speed, there is a threshold value of line energy where maximum weld strength is achieved. These thresholds ensure efficient melting and bonding without causing excessive heat-induced polymer degradation. It is observed that, for the same line energy, the midvalue of the scanning speed used in this study (90 mm/s) yields maximum strength. This speed value may strike a balance, facilitating efficient heat distribution, optimal energy input, reduced cooling effects, and minimal or no degradation, potentially leading to stronger welds. Figure 9(b) shows that higher line energy consistently widens the weld, regardless of scanning speed, but at constant line energy, higher scanning speeds produce broader welds. In LTW, higher line energy broadens the weld width by increasing the melting zone, while higher scanning speeds, when maintaining constant line energy, produce wider welds by mitigating depth-wise heat dissipation.

Figure 10 presents weld strength results alongside corresponding weld width data, revealing a polynomial fit indicating an overall increase in weld strength as weld width expands. Larger weld widths offer greater surface area to withstand shear loads in lap-shear tests, yet this relationship is intricate, and dependent on multiple factors. Notably, some data points show wider welds with reduced strength, attributable to the intricacies of welding quality, heat input, material mixing, and stress distribution. Wider welds may not consistently yield higher strength, as defects or inadequate bonding can undermine them. Moreover, as the weld width increases, the curve depicting strength evolution gradually levels off, suggesting that strength may reach a plateau beyond a specific weld width. This observation implies that there is a limit to the strength improvement achievable solely through widening the weld, reinforcing the idea that other factors must be carefully considered for optimal performance.

6. Fracture Surface Characteristics and Weld Morphology

Fracture surface characteristics in the interface of polymer welds created by LTW are crucial indicators of weld quality and provide valuable insights into the welding process. For the examination of weld morphology, high-magnification images of

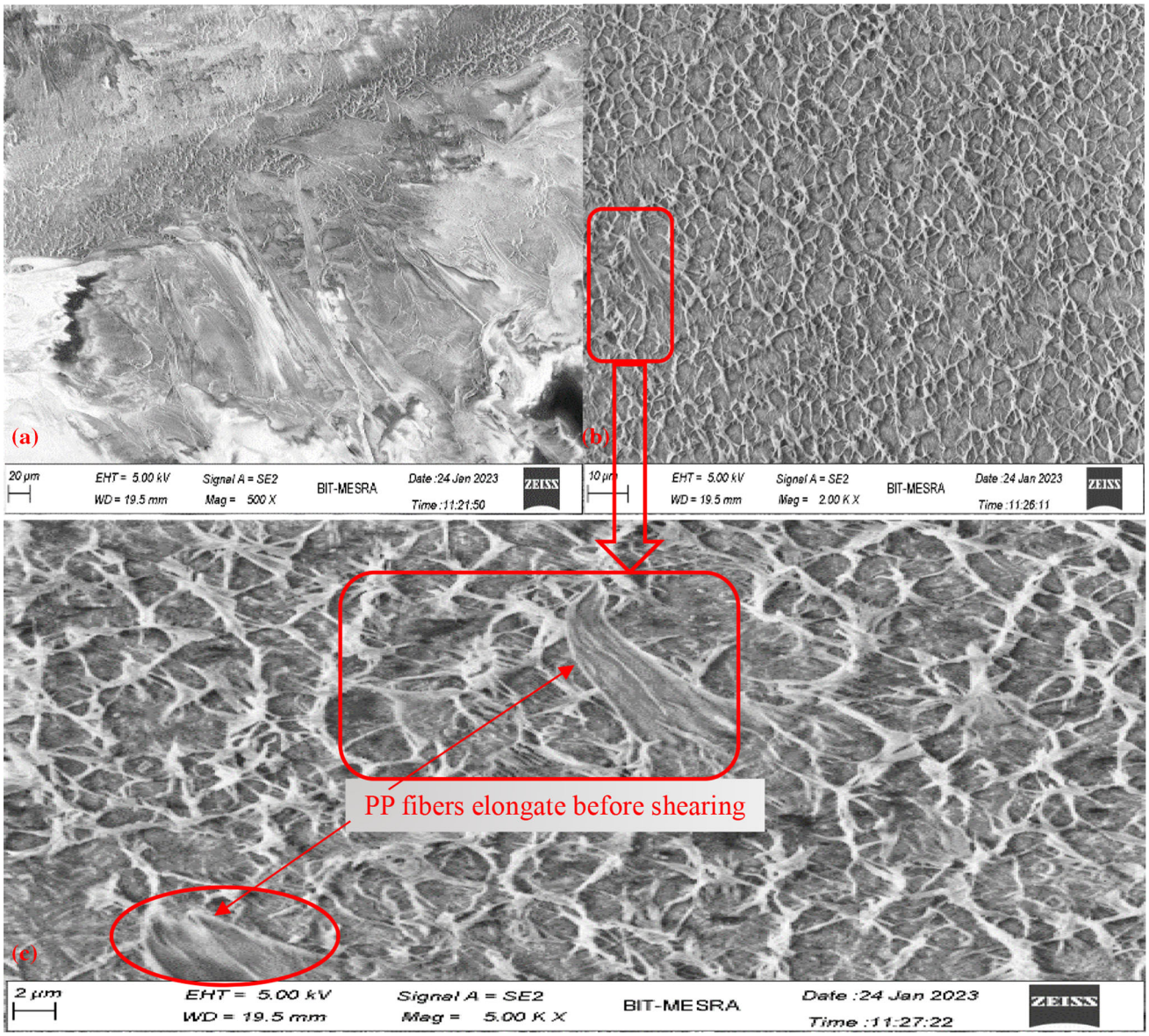

Fig. 11 FESEM images of (a) the interfacial surface of natural PP post-failure, (b) a high-magnification view (2kX) of the interfacial region, and (c) cleavage boundaries at 5kX magnification demonstrating fiber elongation

the weld interface and the weld cross-section of the fractured weld sample are captured using a field emission scanning electron microscope (FESEM). Figure 11(a) depicts the interfacial surface of natural PP within the weld zone post-failure, revealing evident traces of melt flow generated during welding and shear flow resulting from shear testing. Figure 11(b) provides a high-magnification view (2kX) of the interfacial region, prominently demonstrating significant elongation of the PP fibers before tearing at the weld interface due to the adhesion between the joining PP components during LTW. This compellingly demonstrates strong intermolecular bonding and cohesive failure within the weld zone (Ref 53). Further, Fig. 11(c) at 5kX magnification displays cleavage boundaries with strong adhesion due to melting and fusion, initial resistance at cleavage boundaries to joint separation, and subsequent fiber elongation before failure under shear loading. The observed elongation demonstrates the resilience of weld interfaces to mechanical stress, highlighting LTW's success in forming robust intermolecular bonds and cohesive failure within the weld zone.

Figure 12(a) displays the morphology of a particular region at the weld interface on the fracture surface of 0.2% CB-PP at 2kX magnification, while Fig. 12(b) provides a further magnified view at 5kX, offering a more detailed representation of the morphological characteristics seen in Fig. 12(a). The weld zone exhibits a progressive, intra-layer PP fracture mechanism, as evidenced in Fig. 12(a), primarily attributed to the intra-layer mixing of natural PP and CB-PP. This mechanism implies that material layers may endure differing strain and damage levels before ultimate failure (Ref 54). This fracture pattern occurs after the PP fibers at cleavage boundaries have been stretched to their maximum strain, indicating the cohesive nature of the weld (Ref 55). It demonstrates a robust ability to withstand fracture. Figure 12(c) presents the melt pool region on the CB-PP covering the entire melt width, whereas Fig. 12(d) displays a magnified view of a selected

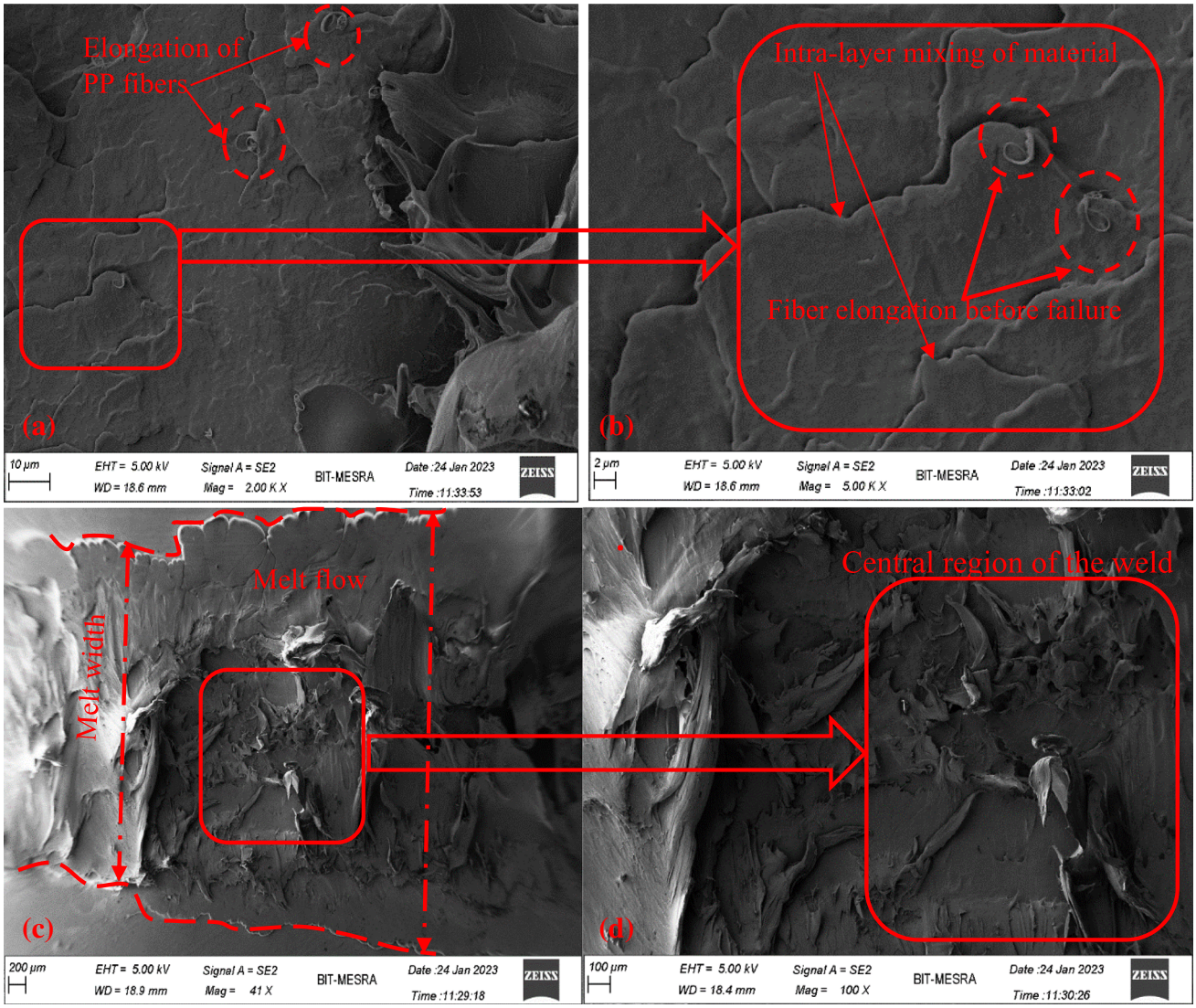

Fig. 12 FESEM images of CB-PP interface: (a) 2kX view of intra-layer fracture mechanism, (b) 5kX magnification for detailed representation, (c) melt pool on CB-PP, and (d) magnified central melt pool region with elongated fibers

portion of the melt pool region at a higher magnification. Higher observed fiber elongations at the central part of the weld seam support the inference that the predominant intermixing of PP layers occurs in this central region, potentially resulting in higher strengths compared to edges of the weld seam where melts inadequately adhere to adjoining polymer plaques. The stretching of PP fibers signifies that material intermixing between the layers enhances the overall strength. This intermingling of materials is a consequence of the elevated temperature at the interface of both polymers, induced by the heat input during welding.

Figure 13(a) provides a FESEM image capturing the cross-sectional view of the weld zone, offering clear visibility of the interface line between the PP (at the top) and CB-PP (at the bottom). This is the weld zone of a duplicate specimen of the weld that failed due to shearing at the weld interface. However, the duplicate specimen is not subjected to shear testing and is solely used for observing the weld cross-section. It is observed that the presence of tiny air gaps alongside areas exhibits thorough fusion in the weld interface (Ref 14). Figure 13(b), when examined at higher magnification, reveals a high-quality fusion within the weld interface, effectively connecting the natural PP with CB-PP in a robust manner. This is notably corroborated by the lack of visible air gaps in the enlarged section of the weld, suggesting that any such gaps that may have existed previously have been effectively sealed through thermal expansion and melt flow during the welding process. No signs of decomposition or voids are apparent at the interface or within the substrate. Figure 13(c) depicts a FESEM image of the weld zone from a duplicate specimen, which failed due to a fracture originating from the base material. In this specimen, the absence of a traceable interfacial line at the weld indicates effective fusion and melt mixing within the weld pool, likely contributing to the high weld strength and the fracture mode observed at the base material. It is also notable that some craters are visible on the cross-section, likely resulting from material chipping during the polishing process. This may be attributed to material degradation in that specific area, possibly caused by excessive heat or pressure or their combined effect (Ref 54). However, partial decomposition has occurred in the weld zone

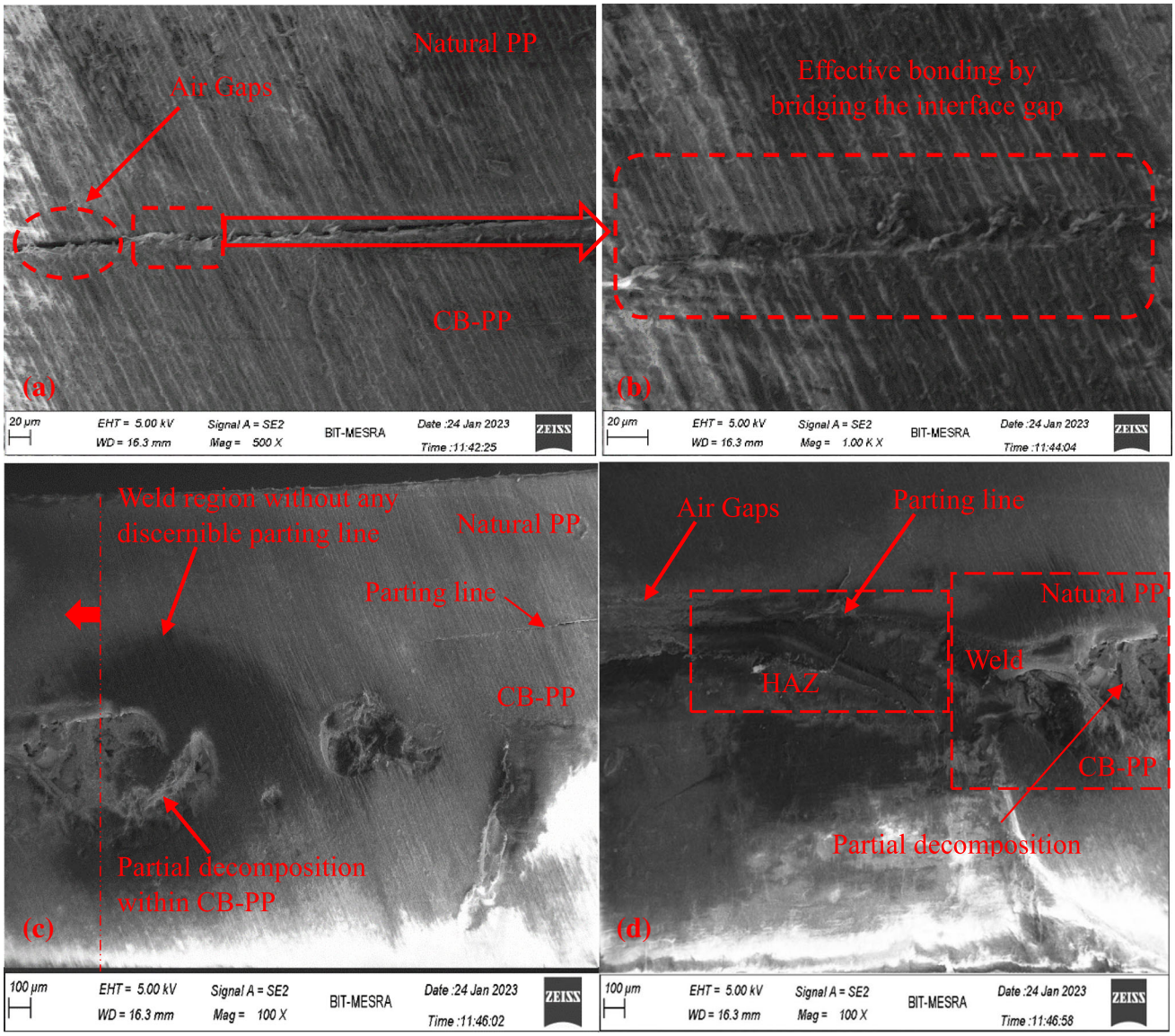

Fig. 13 FESEM image of (a) weld cross-section from a sample with shear failure at the interface, (b) high-magnification image showing fusion zone, (c) weld cross-section from a sample failing in fracture from the base polymer, and (d) cross-sectional view revealing both the weld and HAZ

within CB-PP, primarily where the maximum heat is generated. This is in contrast to the interface, where the available heat is relatively lower due to heat diffusion through contact conduction into natural PP. Figure 13(d) provides a cross-sectional view of the weld zone from the same weld sample, focusing on the left portion of the image in Fig. 13(c) (indicated by an arrow and centerline in Fig 13(c)), which clearly shows both the weld and HAZ, the region adjacent to the weld affected by heat. It is noticeable that while the parting line is not visible within the weld, it becomes apparent in the HAZ (Ref 56, 57).

7. Conclusion

The purpose of this paper is to investigate the LTW of PP and provide a deeper understanding of the LTW process. The investigation involves a thorough analysis of the parametric interplay, evaluation of joint quality, examination of fracture modes in welded structures, and scrutiny of fracture surface characteristics and weld morphology. Based on the material and parameters investigated, the following conclusion can be drawn from this investigation:

1. DSC and TGA data offer crucial insights into polymer thermal behavior, with added carbon black boosting thermal stability and crystallinity in PP.
2. Higher weld strengths corresponded to fractures in the base polymer, while weaker bonding led to failures at the weld interface. Excellent bonding is evident from residue traces.
3. Increasing laser power initially enhances weld strength due to improved fusion, but exceeding the optimal range leads to thermal degradation and weaker welds.
4. Weld strength and width rely on balancing scanning speed and defocus distance, optimizing concentrated heating and sufficient heat absorption.

5. Weld strength increases with defocus distance but diminishes beyond a threshold, while higher laser power consistently enhances strength at higher defocus distances.
6. Optimal line energy control, with higher laser power and faster scanning speed, yields stronger welds, while increased line energy widens welds.
7. The fracture surface characteristics and morphological analysis demonstrate strong interfacial bonding, cohesive failure, and robust weld joints.
8. The lack of visible air gaps, effective fusion, and minimal signs of decomposition in the weld interface contribute to robust weld integrity.

Acknowledgment

The authors gratefully acknowledge the central instrumentation facility (CIF) of BIT Mesra, Ranchi, India, for extending necessary infrastructural support for carrying out testing and characterization of the weld samples.

Author Contributions

GA did investigation, methodology, formal analysis, and writing—original draft. BA done conceptualization, visualization, writing—review & editing, resources, and supervision.

Funding

This research is partially supported by the Science and Engineering Research Board, DST, New Delhi, India, Grant Number CRG/2022/004102.

Data Availability

The data that support the findings of this study are available from the corresponding author, upon reasonable request.

Conflict of interest

The authors declare that they have no known competing financial interests or personal relationships that could have appeared to influence the work reported in this paper.

References

1. B. Acherjee, Laser Transmission Welding of Polymers–A Review on Process Fundamentals, Material Attributes, Weldability, and Welding Techniques, *J. Manuf. Process.*, 2020, **60**, p 227–246
2. V.A. Kagan, Innovations in Laser Welding of Thermoplastics: This Advanced Technology is Ready to be Commercialized. *SAE Trans.*, 2002, p 845–864
3. B. Acherjee, A.S. Kuar, S. Mitra, and D. Misra, Effect of Carbon Black on Temperature Field and Weld Profile During Laser Transmission Welding of Polymers: A FEM Study, *Opt. Laser Technol.*, 2012, **44**(3), p 514–521
4. I.A. Jones and R.J. Wise, Welding Method, Patent WO 00/20157, 1998
5. I. Mingareev, F. Weirauch, A. Olowinsky, L. Shah, P. Kadwani, and M. Richardson, Welding of Polymers Using a 2 μm Thulium Fiber Laser, *Opt. Laser Technol.*, 2012, **44**(7), p 2095–2099
6. G. Anwer and B. Acherjee, Laser Polymer Welding Process: Fundamentals and Advancements, *Mater. Today Proc.*, 2022, **61**, p 34–42
7. P. Lakemeyer and V. Schöppner, Laser Transmission Welding of Automotive Headlamps without a Clamping Tool, *Weld. World*, 2017, **61**, p 589–602
8. B. Acherjee, Laser Transmission Welding of Polymers–a Review on Welding Parameters, Quality Attributes, Process Monitoring, and Applications, *J. Manuf. Process.*, 2021, **64**, p 421–443
9. V.A. Kagan and G.P. Pinho, Laser Transmission Welding of Semicrystalline Thermoplastics-Part II: Analysis of Mechanical Performance of Welded Nylon, *J. Reinf. Plast. Compos.Reinf. Plast. Compos.*, 2004, **23**(1), p 95–107
10. S.A. Kocheny, V.A. Kagan, and J. Macur, Through-transmission Laser Welding of Nylon: Breaking the Moisture Barrier. *ANTEC conference proceedings* (Vol. 1, pp. 1188-1192). Society of Plastics Engineers, 2004
11. V.A. Kagan, S.A. Kocheny, and J.E. Macur, Moisture Effects on Mechanical Performance of Laser-welded Polyamide, *J. Reinf. Plast. Compos.Reinf. Plast. Compos.*, 2005, **24**(11), p 1213–1223
12. R. Prabhakaran, M. Kontopoulou, G. Zak, P.J. Bates, and B.K. Baylis, Contour Laser–laser-Transmission Welding of Glass Reinforced Nylon 6, *J. Thermoplast. Compos. Mater.Thermoplast. Compos. Mater.*, 2006, **19**(4), p 427–439
13. N. Amanat, C. Chaminade, J. Grace, D.R. McKenzie, and N.L. James, Transmission Laser Welding of Amorphous and Semi-crystalline Polyether–ether–ketone for Applications in the Medical Device Industry, *Mater. Des.*, 2010, **31**(10), p 4823–4830
14. E. Rodríguez-Vidal, I. Quintana, and C. Gadea, Laser Transmission Welding of ABS: Effect of CNTs Concentration and Process Parameters on Material Integrity and Weld Formation, *Opt. Laser Technol.*, 2014, **57**, p 194–201
15. V. Mamuschkin, A. Haeusler, C. Engelmann, A. Olowinsky, and H. Aehling, Enabling Pyrometry in Absorber-free Laser Transmission Welding Through Pulsed Irradiation, *J. Laser Appl.*, 2017, **29**(2), p 022409
16. A.B. Pereira, F.A.O. Fernandes, A.B. de Morais, and J. Quintão, Mechanical Strength of Thermoplastic Polyamide Welded by Nd:YAG Laser, *Polymers*, 2019, **11**, p 1381
17. M. Ilie, V. Stoica, E. Cicala, and J.C. Kneip, Experimental Design Investigation of Through-transmission Laser Welding of Dissimilar Polymers, *J. Phys. Conf. Ser.*, 2020, **1426**(1), p 012045
18. D. Kumar, N.S. Sarkar, B. Acherjee, and A.S. Kuar, Beam Wobbling Effects on Laser Transmission Welding of Dissimilar Polymers: Experiments, Modeling, and Process Optimization, *Opt. Laser Technol.*, 2022, **146**, p 107603
19. X. Yu, Q. Long, Y. Chen, Y. Liu, C. Yang, Q. Jia, and C. Wang, Laser Transmission Welding of Dissimilar Transparent Thermoplastics Using Different Metal Particle Absorbents, *Opt. Laser Technol.*, 2022, **150**, p 108005
20. Y. Liu, W. Zhang, J. Liu, Y. Guan, and X. Ding, Study on Microstructures and Mechanical Performance of Laser Transmission Welding of Poly-ether-ether-ketone (PEEK) and Carbon Fiber Reinforced PEEK (CFR-PEEK), *J. Laser Appl.*, 2022, **34**(4), p 042037
21. X. Wang, X. Song, M. Jiang, P. Li, Y. Hu, K. Wang, and H. Liu, Modeling and Optimization of Laser Transmission Joining Process Between PET and 316L Stainless Steel Using Response Surface Methodology, *Opt. Laser Technol.*, 2012, **44**(3), p 656–663
22. U. Nath and V. Yadav, Analytical Modeling of Temperature Evolution and Bend Angle in Laser Forming of Al 6061–T6 Sheets and its Experimental Analysis, *Opt. Laser Technol.*, 2022, **154**, p 108307
23. V. Kumar, U.S. Dixit, and J. Zhang, Determining Thermal Conductivity, Specific Heat Capacity and Absorptivity During Laser Based Materials Processing, *Measurement*, 2019, **139**, p 213–225
24. U. Nath and V. Yadav, Inverse Model for Simultaneously Estimating Material Parameters and Absorption Coefficient in a Laser-irradiated Sheet, *Lasers Manuf. Mater. Process.*, 2023, **10**(4), p 606–625
25. L.S. Mayboudi, A.M. Birk, G. Zak, and P.J. Bates, Laser Transmission Welding of a Lap-joint: Thermal Imaging Observations and Three–dimensional Finite Element Modeling, *J. Heat Transfer*, 2007, **129**, p 1177–1186
26. B. Acherjee, 3-D FE Heat Transfer Simulation of Quasi-simultaneous Laser Transmission Welding of Thermoplastics, *J. Braz. Soc. Mech. Sci. Eng.*, 2019, **41**(10), p 466

27. A. Schkutow and T. Frick, Influence of Adapted Wavelengths on Temperature Fields and Melt Pool Geometry in Laser Transmission Welding, *Phys. Procedia*, 2016, **83**, p 1055–1063
28. P. Lakemeyer and V. Schöppner, Simulation-based Investigation on the Temperature Influence in Laser Transmission Welding of Thermoplastics, *Weld. World*, 2019, **63**(2), p 221–228
29. C. Wang, H. Liu, Z. Chen, D. Zhao, and C. Wang, A New Finite Element Model Accounting for Thermal Contact Conductance in Laser Transmission Welding of Thermoplastics, *Infrared Phys. Technol.*, 2021, **112**, p 103598
30. R. Prabhakaran, M. Kontopoulou, G. Zak, P. Bates, and V. Sidiropoulos, Simulation of Heat Transfer in Laser Transmission Welding, *Int. Polym. Proc.Polym. Proc.*, 2005, **20**(4), p 410–416
31. B. Acherjee, Numerical Study of Thermo-mechanical Responses in Laser Transmission Welding of Polymers Using a 3-D thermo-elasto-viscoplastic FE Model, *Weld. World*, 2022, **66**(7), p 1421–1435
32. D.K. Goyal, R. Yadav, and R. Kant, An Integrated Hybrid Methodology for Estimation of Absorptivity and Interface Temperature in Laser Transmission Welding, *Int. J. Adv. Manuf. Technol.*, 2022, **121**(5–6), p 3771–3786
33. X.F. Xu, A. Parkinson, P.J. Bates, and G. Zak, Effect of Part Thickness, Glass Fiber and Crystallinity on Light Scattering During Laser Transmission Welding of Thermoplastics, *Opt. Laser Technol.*, 2015, **75**, p 123–131
34. H. Ghasemi, Y. Zhang, P.J. Bates, G. Zak, and D.L. DuQuesnay, Effect of Processing Parameters on Meltdown in Quasi-simultaneous Laser Transmission Welding, *Opt. Laser Technol.*, 2018, **107**, p 244–252
35. Z. Chen, Y. Huang, F. Han, and D. Tang, Numerical and Experimental Investigation on Laser Transmission Welding of Fiberglass-doped PP and ABS, *J. Manuf. Process.*, 2018, **31**, p 1–8
36. N.P. Nguyen, S. Behrens, M. Brosda, A. Olowinsky, and A. Gillner, Laser Transmission Welding of Absorber-free semi-crystalline Polypropylene by Using a Quasi-simultaneous Irradiation Strategy, *Weld. World*, 2020, **64**, p 1227–1235
37. M.L. Röhricht, T. Stichel, S. Roth, P.A.B. Bräuer, M. Schmidt, and S. Will, Correlation Between Weld Seam Morphology and Mechanical Properties in Laser Transmission Welding of Polypropylene, *Procedia CIRP*, 2020, **94**, p 691–696
38. M.M. Ali, F. Dave, R. Sherlock, A. Mcilhagger, and D. Tormey, Simulated Effect of Carbon Black on High Speed Laser Transmission Welding of Polypropylene With Low Line Energy, *Front. Mater.*, 2021, **8**, p 737689
39. F. Dave, M.M. Ali, M. Mokhtari, R. Sherlock, A. McIlhagger, and D. Tormey, Effect of Laser Processing Parameters and Carbon Black on Morphological and Mechanical Properties of Welded Polypropylene, *Opt. Laser Technol.*, 2022, **153**, p 108216
40. S. Hammani, N. Moulai-Mostefa, P. Samyn, M. Bechelany, A. Dufresne, and A. Barhoum, Morphology, Rheology and Crystallization in Relation to the Viscosity Ratio of polystyrene/polypropylene Polymer Blends, *Materials*, 2020, **13**(4), p 926
41. P. Verma and V. Choudhary, Polypropylene Random Copolymer/MWCNT Nanocomposites: Isothermal Crystallization Kinetics, Structural, and Morphological Interpretations, *J. Appl. Polym. Sci.Polym. Sci.*, 2015, **132**(13), p 41734
42. R. Ma, B. Zhu, Q. Zeng, P. Wang, Y. Wang, C. Liu, and C. Shen, Melt-Processed Poly (ether ether ketone)/Carbon Nanotubes/Montmorillonite Nanocomposites with Enhanced Mechanical and Thermomechanical Properties, *Materials*, 2019, **12**(3), p 525
43. V. Rangari and J. Davis, Thermal and Mechanical Properties of Polypropylene Polymer Nanocomposites Infused with Sonochemically Coated SiC/SiO_2 Nanoparticles. *Composite Materials*, IntechOpen, 2020
44. R. Nasrin, M.A. Gafur, and A.H. Bhuiyan, Characterization of Isotactic Polypropylene/Talc Composites Prepared by Extrusion Cum Compression Molding Technique, *Mater. Sci. Appl.*, 2015, **6**(11), p 925
45. X. Wang, H. Chen, and H. Liu, Investigation of the Relationships of Process Parameters, Molten Pool Geometry and Shear Strength in Laser Transmission Welding of Polyethylene Terephthalate and Polypropylene, *Mater. Des.*, 2014, **55**, p 343–352
46. R.K. Nath, V. Jha, P. Maji, and J.D. Barma, A Novel Double-Side Welding Approach for Friction Stir Welding of Polypropylene Plate, *Int. J. Adv. Manuf. Technol.*, 2021, **113**, p 691–703
47. A.B. Pereira, F.A. Fernandes, A.B. de Morais, and J. Quintão, Mechanical Strength of Thermoplastic Polyamide Welded by Nd: YAG Laser, *Polymers*, 2019, **11**(9), p 1381
48. P. Bates, M. Druart, M. Chen, G. Zak, and J. Billiet, Influence of Part Thickness, Glass Fibre Content and Line Energy on Laser Transmission Welding of Polyamide mXD6, *ANTEC- Conf. Proc.*, 2007, **5**, p 2766
49. A. Gisario, F. Veniali, M. Barletta, V. Tagliaferri, and S. Vesco, Laser Transmission Welding of Poly (ethylene terephthalate) and Biodegradable Poly (ethylene terephthalate)–based Blends, *Opt. Lasers Eng.*, 2017, **90**, p 110–118
50. A. Jansson, S. Kouvo, A. Salminen, and V. Kujanpää, The Effect of Parameters on Laser Transmission Welding of Polymers. In *International Congress on Applications of Lasers & Electro-Optics*. AIP Publishing, 2003
51. B. Acherjee, D. Misra, D. Bose, and K. Venkadeshwaran, Prediction of Weld Strength and Seam width for Laser Transmission Welding of Thermoplastic Using Response Surface Methodology, *Opt. Laser Technol.*, 2009, **41**(8), p 956–967
52. B. Acherjee, A.S. Kuar, S. Mitra, and D. Misra, Finite Element Simulation of Laser Transmission Thermoplastic Welding of Circular Contour Using a Moving Heat Source, *Int. J. Mechatron. Manuf. Syst.*, 2013, **6**(5–6), p 437–454
53. A. Baldan, Adhesively-bonded Joints in Metallic Alloys, Polymers and Composite Materials: Mechanical and Environmental Durability Performance, *J. Mater. Sci.*, 2004, **39**, p 4729–4797
54. X. Wang, B. Liu, W. Liu, X. Zhong, Y. Jiang, and H. Liu, Investigation on the Mechanism and Failure Mode of Laser Transmission Spot Welding Using PMMA Material for the Automotive Industry, *Materials*, 2017, **10**(1), p 22
55. Ö. Yağci, B. EkerGümüş, and M. Taşdemir, Thermal, Structural and Morphological Properties of Polypropylene and High Density Polyethylene Polymer Composites Filled with Waste Urea Formaldehyde, *Polym. Bull.. Bull.*, 2023, **80**(4), p 4005–4022
56. M. Cakmak, J. Robinette, and S. Schaible, Structure Development and Dynamics of Vibration Welding of Poly (ethylene naphthalate) from Amorphous and Semicrystalline Precursors, *J. Appl. Polym. Sci.Polym. Sci.*, 1998, **70**(1), p 89–108
57. Y.M. Chung and M.R. Kamal, Morphology of PA-6 Vibration Welded Joints and its Effect on Weld Strength, *Polym. Eng. Sci.. Eng. Sci.*, 2008, **48**(2), p 240–248